Title
Geometry and field dependence of the Fermi surface in TiBe2 studied with the DHVA effect in fields up to 35 T

Journal
Journal of Physics F Metal Physics, 14(11)

ISSN
0305-4608

Authors
van Ruitenbeek, JM
van Deursen, APJ
Schreurs, LWM
et al.

Publication Date
1984-11-01

DOI
10.1088/0305-4608/14/11/013

J. Phys. F: Met. Phys. **14** (1984) 2555–2569. Printed in Great Britain

Geometry and field dependence of the Fermi surface in $TiBe_2$ studied with the DHVA effect in fields up to 35 T

J M van Ruitenbeek†, A P J van Deursen†, L W M Schreurs†, R A de Groot†, A R de Vroomen†, Z Fisk‡ and J L Smith‡

† Fysisch Laboratorium, Katholieke Universiteit, Toernooiveld 1, 6525 ED Nijmegen, The Netherlands

‡ Los Alamos National Laboratory, Los Alamos, New Mexico 87545, USA

Received 3 January 1984, in final form 10 April 1984

Abstract. The DHVA effect in single crystals of $TiBe_2$ has been investigated in magnetic fields between 10 and 35 T using a pulsed-field system. Two sheets of Fermi surface are found, an electron sheet around Γ and an X-centred hole sheet. Both are split into a majority-spin (↑) and a minority-spin (↓) surface. In the field region studied $\Delta F = F_\uparrow - F_\downarrow$ amounts to about 200 T or 10% of the average frequency values. With the field direction parallel to [110] the field dependence of the splitting of the Γ orbit is studied in detail. It is found that the difference in spin-up and spin-down Fermi surface areas is directly proportional to the magnetisation, within the experimental error. This is in agreement with the Stoner model. Departures from this model due to spin fluctuations are expected below 10 T. The effective masses of the Γ and X orbits show large enhancements of about $\lambda = 3$ and 1.5 respectively.

1. Introduction

Since the discovery of itinerant magnetism in $TiBe_2$ by Matthias *et al* (1978) much work has been devoted to the properties of this exceptional material. It has a very high susceptibility $\chi = M/H$, a factor of 13 larger than that of palladium. $\chi(H)$ and $\chi(T)$ both show a maximum, at 5.5 T and 10 K respectively (Monod *et al* 1980, Acker *et al* 1981a, b, 1982). The low-temperature specific heat shows a pronounced upturn with decreasing temperature which is suppressed in high magnetic fields. This suppression starts at 5.2 T and is complete at about 25 T (Stewart *et al* 1982a, b). Substitution of small amounts of Cu for Be causes the material to become ferromagnetic (Giorgi *et al* 1979).

$TiBe_2$ is generally described as a strongly exchange-enhanced paramagnetic or nearly ferromagnetic metal. The maximum in the susceptibility has been ascribed to spin fluctuations (Acker *et al* 1981b) and this picture is supported by specific heat data (Stewart *et al* 1982a, b). However other explanations for the maximum exist, such as a pronounced structure in the density of states (DOS) near the Fermi energy (Wohlfarth 1981, Jarlborg *et al* 1983) which was also suggested by Alloul and Mihaly (1982) from NMR measurements. In addition $TiBe_2$ has been considered a good candidate to show itinerant metamagnetism (Wohlfarth 1980) and p-state superconductivity (Enz and Matthias 1979).

In this work we present de Haas–van Alphen (DHVA) measurements on single-crystalline $TiBe_2$. The frequencies detected are described by a Γ-centred electron sheet and an X-centred hole sheet. In high fields the Fermi surfaces for the majority and minority

spins are clearly split. The mean frequencies $\bar{F} = \frac{1}{2}(F_\uparrow + F_\downarrow)$ are in good agreement with the results of band-structure calculations (de Groot *et al* 1980, Jarlborg and Freeman 1980, Jarlborg *et al* 1981). Here a refinement is applied to the model of de Groot *et al* for a better comparison with the experiments. The spin splitting of the Fermi surface is observed to be strongly field dependent and the field dependence is compared with the magnetisation of the material. High values for the mass enhancement are found, in agreement with the specific heat data of Stewart *et al* (1982b).

2. Experimental procedure

Since $TiBe_2$ forms peritectically at 1350 °C an off-stoichiometric mixture $Ti_{0.38}Be_{0.62}$ was used to grow the sample. The mixture was cooled down from 1480 °C at 4 °C h^{-1} in a BeO crucible. A single crystal was subsequently separated mechanically. Laue patterns taken from different sides showed no evidence for inclusions of differently oriented crystallites or other phases. The single crystal was spark cut into three small bars, of typical dimensions $0.7 \times 0.7 \times 2.0\ mm^3$, with their long axes along the three principal symmetry axes.

The residual resistivity ratio measured on one of the bars with a standard four-probe method gave $\rho(293\ K)/\rho(4.2\ K) = 26$ and a resistivity at 4.2 K of $\rho = 4 \times 10^{-8}\ \Omega\ m$. The magnetisation was measured on a piece of the single crystal in a Bitter magnet of the Nijmegen high-field facility with fields up to 14.2 T using a moving-sample magnetometer. The zero-field volume susceptibility at 4.2 K is $\chi_0 = M/H = 5.97 \times 10^{-3}$ (this corresponds to 0.96×10^{-2} EMU mol^{-1}) increasing by 17% in a field of 6 T. An Arrott plot of the magnetisation data is shown in figure 1.

In order to be able to compare the splitting of the DHVA frequencies in high fields with the magnetisation we need the latter for this material at 1.3 K in fields up to 32 T. Starting

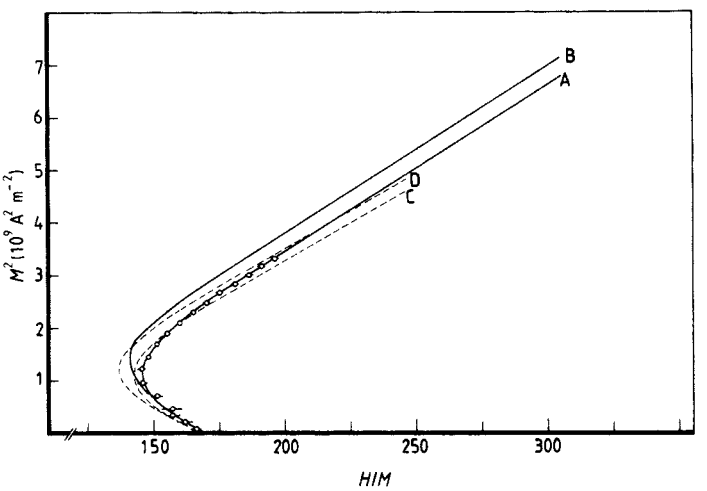

Figure 1. The magnetisation of the single-crystalline sample of $TiBe_2$ up to 14.2 T at 4.2 K (O). The data are extrapolated up to 32 T assuming a linear behaviour above 10 T (A). A correction for the temperature dependence of the magnetisation gives a parallel Arrott plot at 1.3 K (B). For comparison the data of Acker *et al* (1982) for polycrystalline material up to 21.3 T are given at 4.17 K (C) and at 1.45 K (D). We use $B = \mu_0 (H + M)$, so H/M has no dimension.

from the magnetisation measurements at fields up to 14.2 T we use the fact that the Arrott plot is linear from 10 T up to at least 21 T (Acker *et al* 1982) to extrapolate the data, assuming linearity up to 32 T (figure 1). This assumption requires justification with high-field magnetisation measurements. To correct for the temperature dependence the magnetisation is measured between 4.2 and 10 K and extrapolated to 1.3 K giving a 2.5% correction at 10 T with respect to the 4.2 K values, in agreement with the findings of Acker *et al* (1982). Pulsed high-field magnetisation measurements at low temperatures are in preparation.

The DHVA data are taken in a 40 T pulsed-field system. The experimental procedure, amplitude and phase analysis in this system have been described previously (van Ruitenbeek *et al* 1982, van Deursen and de Vroomen 1984).

3. Geometry of the Fermi surface

Figure 2 shows the results for the observed DHVA frequencies as a function of orientation. All data are taken using pulses of maximum field value 35 T and a temperature of 1.3 K. The correction for the contribution to the field from the magnetisation of the sample is less than 1% and is neglected throughout. For most of the field directions, up to 16 single

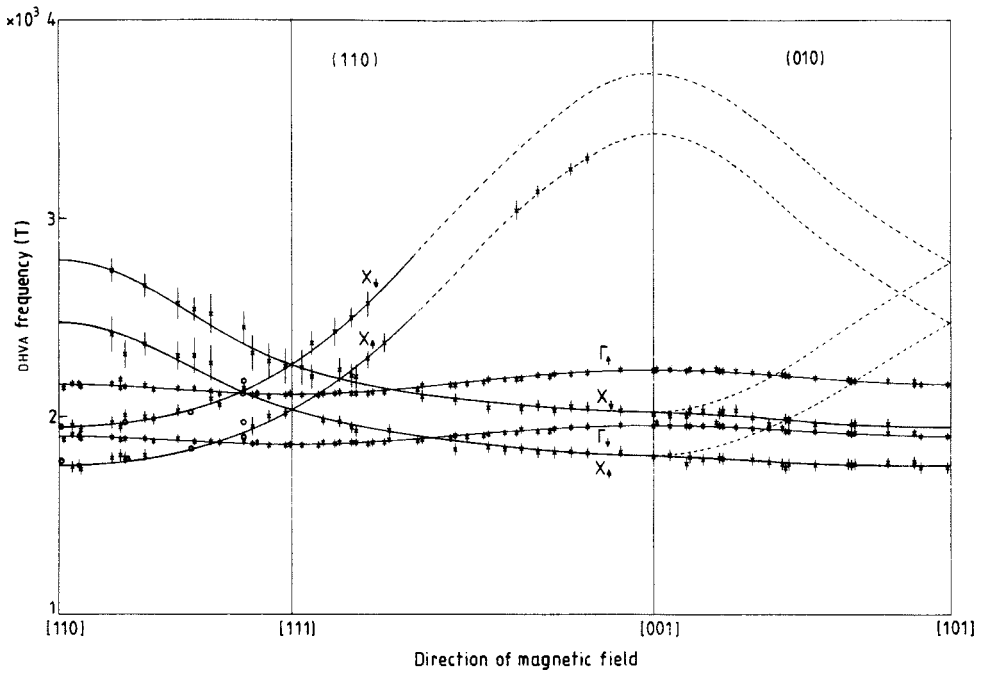

Figure 2. Results for the angular dependence of the DHVA frequencies in $TiBe_2$. All data are taken at 1.3 K using pulses of 35 T top field. Full curves are drawn as a guide to the eye; the broken curves indicate the expected behaviour. Each frequency branch is labelled with the name of the symmetry point in the Brillouin zone forming the centre of the corresponding sheet of Fermi surface. For both the X and Γ sheets there is a majority- (↑) and a minority-spin (↓) branch. The vertical lines through the data points indicate the experimental error. The angles are accurate to 1°. The data of van Deursen *et al* (1982) are also included (open circles).

recordings are accumulated in order to improve the signal-to-noise ratio for the low-amplitude spectral features. The frequencies given are obtained from a Fourier power spectrum of the data. A typical spectrum is shown in figure 3. In figure 2 full curves, drawn on the basis of continuity of amplitude and frequency in the spectra, are given for visual clarity. Broken curves indicate the expected behaviour on the basis of the interpretation given below.

Three sets of nearly parallel branches can be identified, indicating a spin-split Fermi surface. In all measured orientations the amplitude of the branch indicated by $\Gamma_\downarrow$ is strongest, followed by $\Gamma_\uparrow$; both show only a slight angular dependence in frequency and amplitude. The signals clearly originate from a closed part of the Fermi surface with single multiplicity. They are interpreted as spin-split orbits on the nearly spherical Γ-centred electron sheet found in both band-structure calculations (Jarlborg *et al* 1981, de Groot *et al* 1980), Γ_{10} in the notation of de Groot *et al*. For most of the field orientations the second harmonic of $\Gamma_\downarrow$ is also detected.

Several nearly parallel branches of signals with smaller amplitude are also observed, showing a stronger angular dependence. They are attributed to orbits on a spin-split X-centred hole surface (X_7 in de Groot *et al* 1980) and are indicated by $X_\uparrow$ ($X_\downarrow$) for the majority (minority) surface. The X branches that can be followed in the entire $(1\bar{1}0)$ plane are doubly degenerate, as evidenced by the observation of an additional splitting of each branch when the sample is oriented more than 2° out of the plane of rotation.

The amplitude of the X branches decreases with increasing DHVA frequency. The higher frequencies of the X sheet between [110] and [111] are found in the Fourier spectrum as broad shallow maxima (figure 3). This is caused by a strong exponential decay due to the high value of the Dingle temperature. No frequencies are detected along the broken curves except for the four isolated data points near [001]. These are found in two different pieces cut from the single crystal indicating that they are indeed intrinsic $TiBe_2$ frequencies. They are tentatively ascribed to the $X_\uparrow$ sheet. Since the X-frequency branches in the (010) plane can be followed continuously we find that both X sheets remain closed in fields up to about 22 T. In the calculations of Jarlborg *et al* (1981), however, the $X_\downarrow$ sheet forms necks merging into the neighbouring X sheets. The frequencies observed by van

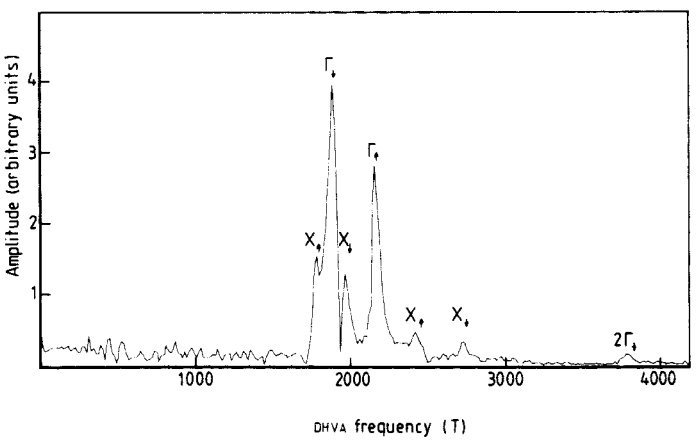

Figure 3. A typical Fourier spectrum of a DHVA recording. The orientation of the field is 8° from [110] towards [111]. The individual points in the Fourier spectrum are connected by a full curve for visual clarity.

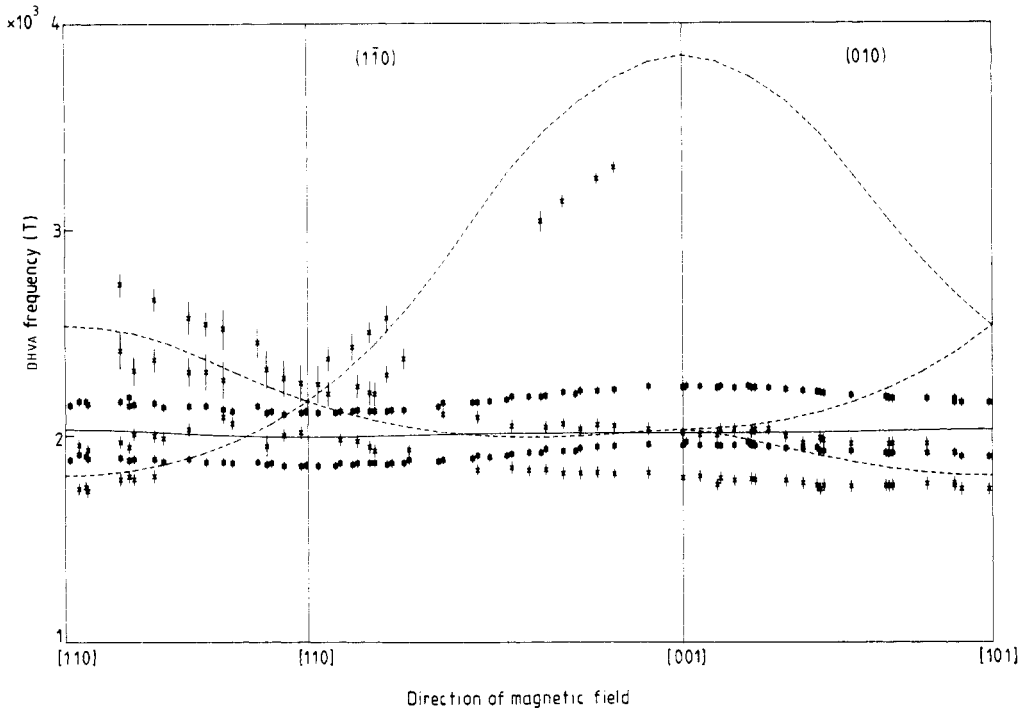

Figure 4. The DHVA frequencies from the band-structure calculation including a non-muffin-tin correction using the experimental data: Γ_{10} (full curve) and X_7 (broken curves). The data from the DHVA experiment are represented by □ for the Γ orbit and × for the X orbit.

Deursen *et al* (1982)† are included in figure 2 and are found to be in good agreement with the present work.

Special attention must be given to interpreting the Fourier spectra because the splitting of DHVA frequencies is field dependent, as discussed in more detail below. The data in figure 2 correspond to the positions of the maxima in the spectra. They represent the DHVA frequencies at some average field value, the average depending on the exponent of decay of each separate frequency. All data are taken using pulses of 35 T top field and are analysed between 31.4 and 9.8 T. The field corresponding to the splitting shown in figure 2 is estimated to be about 22 T. However, an estimation shows that the field dependence of the average of the spin-up and spin-down frequencies $\bar{F}$ can be ignored, and $\bar{F}$ is therefore more accurately determined by the data of figure 2.

For an accurate comparison of the band mass m_b and the effective mass m^* the shape and size of the calculated Fermi surface must be brought into closer agreement with experiment. This was performed as described in the appendix. The resulting angular dependence of the calculated DHVA frequencies is plotted in figure 4 together with the experimental data.

The data presented can be described by two spin-split Fermi surface sheets and the averages of up and down frequencies are in good agreement with the result of the band-structure calculations (Jarlborg *et al* 1981, de Groot *et al* 1980). Given the high values for

† The spectra in figure 1 of this reference are erroneously stated to be measured from [110] towards [100]; this must be [110] towards [111]. The calculated curve remains essentially the same.

Table 1. Fermi surface parameters for the observed Γ-centred and X-centred orbits in $TiBe_2$. The measured frequencies are recorded from the Fourier spectra and correspond to the values at an effective field of about 22 T.

Direction of magnetic field	Branch index	$F_m(10^3$ T) (experimental)		$\bar{F}_m(10^3$ T)		$\Delta F_m(10^3$ T) (experimental)[c]	ΔE (mRyd)[d]
		Majority	Minority	Experimental[a]	Calculated[b]		
[100]	Γ	2.24 ± 0.02	1.96 ± 0.02	2.10 ± 0.03	2.01	0.28 ± 0.03	6.7 ± 0.8
	X	2.01 ± 0.03	1.80 ± 0.03	1.91 ± 0.05	2.03	0.21 ± 0.03	3.7 ± 0.6
	X				3.85		
[111]	Γ	2.11 ± 0.02	1.86 ± 0.02	1.99 ± 0.03	1.99	0.25 ± 0.03	6.4 ± 0.8
	X	2.27 ± 0.08	2.04 ± 0.04	2.16 ± 0.09	2.17	0.23 ± 0.08	5.0 ± 1.8
[110]	Γ	2.16 ± 0.02	1.90 ± 0.02	2.03 ± 0.03	2.03	0.26 ± 0.03	6.3 ± 0.7
	X	1.95 ± 0.03	1.75 ± 0.03	1.85 ± 0.05	1.81	0.20 ± 0.05	5.4 ± 1.4
	X				2.54		

Direction of magnetic field	Branch index	m^* (experimental) Majority	Minority	$\bar{m}^*$ Experimental[a]	m_b Calculated[b]	λ[c]	dm_b/dE (Ryd^{-1})[f]	Δm^* [g]
[100]	Γ	> 2.6	2.2 ± 0.2	> 2.3	0.62	> 2.7	+ 17	> 0.34
	X				0.85		− 10	
	X				1.17		+ 2.9	
[111]	Γ	2.7 ± 0.3	2.1 ± 0.3	2.4 ± 0.5	0.58	3.1 ± 0.9	+ 11	0.29 ± 0.08
	X				0.68		− 4.3	
[110]	Γ	2.5 ± 0.3	2.0 ± 0.3	2.3 ± 0.5	0.61	2.7 ± 0.9	+ 13	0.31 ± 0.09
	X	1.0 ± 0.5			0.55	0.9 ± 0.9	− 4.3	0.02 ± 0.01
	X				0.92		− 2.0	

[a] The average of the experimental values for up and down spin.

[b] From the refined spin-unpolarised band calculation.

[c] The measured frequency difference $\Delta F_m = |F_\uparrow - F_\downarrow|$.

[d] The total energy shift is estimated from $\Delta E = (2\mu_B \Delta F_m / m_b)(M/M_1)$ for M and M_1 at 22 T. The quantity M_1 is introduced in § 6.2.

[e] The mass enhancement $\lambda = \bar{m}^*/m_b - 1$.

[f] The energy dependence of m_b has been derived from the refined band calculation.

[g] The difference between spin-up and spin-down effective masses is estimated using $\Delta m^* = (1 + \lambda)(dm_b/dE)\Delta E$.

the susceptibility and electronic specific heat, there must be additional sheets of the Fermi surface. These are present in the calculations but have such high effective masses that they are not seen in the DHVA experiment.

4. Effective masses

The effective masses are determined from the change in amplitude of the DHVA signals between 1.3 and 2.1 K. The signal between 31.4 and 9.8 T at 1.3 K was divided by the temperature-dependent term in the Lifshitz–Kosevich formula corresponding to this temperature and with an assumed value for the effective mass. Subsequently this signal was multiplied by a term corresponding to $T = 2.1$ K and the Fourier spectrum of the result was compared with that of the 2.1 K data. This procedure was iterated for different estimates of m^* and in this way the correct value of and the error in m^* were obtained. If the effective masses are field dependent, the value thus obtained corresponds to a field between 31.4 and approximately 22 T. The results are given in table 1. The value for $X_\uparrow$ along [110] is in agreement with the value observed earlier by van Deursen *et al* (1982). The band masses calculated from the refined model described in the appendix and values for the mass enhancement λ are also given in table 1. The values for λ are high, especially for the Γ orbit.

From the refined band-structure calculation a value for the derivative of the band mass with respect to the energy is obtained (table 1). Using this band value and the energy splitting (table 1), which will be discussed later, a value for the difference in effective mass for the two spin directions is estimated as

$$\Delta m^* = (1 + \lambda)(\mathrm{d}m_b/\mathrm{d}E)\Delta E$$

where m_b is the bare band mass and ΔE is the exchange splitting. The results are also given in table 1 and are in agreement with the experiment.

High values for the mass enhancement have been observed previously in weak itinerant magnetic systems using the DHVA effect, for example in $ZrZn_2$ by van Ruitenbeek *et al* (1982) and in Ni_3Al by Lonzarich *et al* (1983). The mass enhancement found from the specific heat for $TiBe_2$ is also high. From the specific heat measurements of Stewart *et al* (1982a) a value of $\lambda = 3.6$ is derived in zero field by comparing the electronic specific heat with the band-structure value for the density of states at the Fermi level of $N(E_F) = 34$ states $\mathrm{Ryd}^{-1}\ \mathrm{spin}^{-1}\ \mathrm{FU}^{-1}$ (FU = formula unit) from the refined band calculation. If a field is applied, the value of the electronic specific heat γ decreases (Stewart *et al* 1982a) and accordingly λ decreases. One may also expect that, apart from the non-parabolic band effects resulting in a different mass for the two spin directions, the average of spin-up and spin-down effective masses is field dependent. Therefore the values for the mass enhancement can be compared only if they are determined at the same field strength.

The effective masses are determined for a field of about 22 T or higher. Assuming a 25% decrease for γ at this field we find a value $\lambda = 2.5$ from the high-field specific heat data. This estimate is in good agreement with the values of λ for the Γ orbit listed in table 1. However, the specific heat is dominated by the bands with a high partial density of states $N(E_F)$, not seen in DHVA; the observed Γ sheet contributes only a small fraction to the total $N(E_F)$. Note that the light bands observed here show a mass enhancement of comparable magnitude.

5. Dingle temperatures

From the change in amplitude of the beat maxima of the total signal with field a Dingle temperature is estimated for the Γ orbits. The contributions of the X frequencies to the total signal are ignored. The Dingle plots show no apparent deviations from linearity. The resulting values for the three pieces of the single crystal are in the range $(2.3 \pm 0.5)\ \mathrm{K} < m^* T_D^* < (3.7 \pm 0.5)\ \mathrm{K}$. The difference in amplitude of the Γ oscillations for the two spin directions (figure 3) corresponds to a difference in Dingle temperature of $(20 \pm 10)\%$. From the Fourier spectra taken over different field ranges, a Dingle temperature for $X_\uparrow$ along [110] of $m^* T_D^* = 6$ K was estimated.

6. Field dependence of the Fermi surface

In itinerant paramagnetic or ferromagnetic materials the Fermi surface changes as a function of the magnetisation. The Fermi surface for the minority-spin electrons shrinks and the majority surface expands with increasing applied field. For paramagnetic metals this is commonly described by a cosine factor in the Lifshitz–Kosevich formula for the DHVA effect (Gold 1968). This cosine factor is constant if the susceptibility, and consequently the Stoner factor, is field independent. If the susceptibility shows some field dependence this will result in an additional field dependence of the DHVA amplitude and even 'spin-splitting zeros' may be observed at some field value. For materials like $TiBe_2$ showing a very strong field dependence of the susceptibility, the number of observed spin-splitting zeros is large and the DHVA effect is better described by two separate field-dependent frequencies. A strong field dependence of the Fermi surface was also observed for the weak itinerant ferromagnet $ZrZn_2$ (van Ruitenbeek *et al* 1982).

6.1. Experimental results

With the field in the [110] direction, accurate DHVA data are recorded. Fourier spectra taken over different field ranges clearly show a field dependence of the Γ frequencies and of the $X_\uparrow$ frequency. The $X_\downarrow$ frequency is hidden under the stronger $\Gamma_\downarrow$ peak. The amplitude of the X frequencies is only 10% of the amplitude of the Γ frequencies. For the moment we ignore the X frequencies and analyse the field dependence of the Γ frequencies by fitting two exponentially damped sine functions over parts of the data. The intervals were chosen to contain two periods of the frequency difference ΔF. In figure 5 the results for the frequency difference measured in fields between 11.0 and 30.4 T, here labelled ΔF_m, are plotted against B. The ΔF_m values are obtained from pulses of 35, 26 and 18 T top field; good agreement is found between the corresponding data from these different pulses, and the average values are given in figure 5.

The assumption that the X frequencies can be ignored was monitored as follows. A computer program simulated the DHVA signals for the Γ and X orbits, including a field-dependent frequency, in close analogy to the measured signals. Fitting the simulated data with two frequencies reproduced the correct frequency difference except for the highest field values. The error bars in figure 5 show this systematic error.

6.2. Comparison of ΔF with the magnetisation

In figure 6(*a*) the values for ΔF_m are plotted as a function of the magnetisation M. The

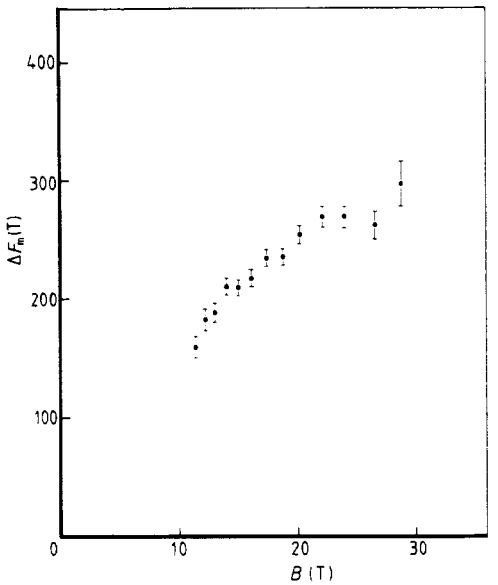

Figure 5. Results for the measured difference in frequency ΔF between $\Gamma_\uparrow$ and $\Gamma_\downarrow$ plotted as a function of the magnetic field strength.

broken line results from the band-structure calculation by shifting the two spin sub-bands rigidly up and down. The discrepancy between the ΔF_m values and the calculated line is due primarily to the 'Doppler' shift in the DHVA effect (van Ruitenbeek *et al* 1982).

Since both the Fermi surface and the Landau levels are changing with field, the DHVA frequencies do not follow the Onsager relation. Instead we measure a momentary frequency F_m given by

$$F_m(B) = \mathrm{d}(F(B)/B)/\mathrm{d}B^{-1} = F(B) - B(\mathrm{d}F(B)/\mathrm{d}B) \tag{1}$$

where $F(B)$ is the frequency related by the Onsager equation

$$F = (\hbar/2\pi e)A \tag{2}$$

to the extremal cross-sectional area A of the Fermi surface. One is interested in the extremal cross sections, so the measured frequencies must be corrected for this 'Doppler' shift. By integration of equation (1) $F(B)$ cannot be recovered uniquely since replacement of $F(B)$ by $F(B) + cB$ for any constant c gives the same $F_m(B)$. Therefore we use a different approach concentrating on the difference between spin-up and spin-down frequencies ΔF and starting with an expression for $\Delta F(B)$. We assume that in fields above 10 T the magnetisation of $TiBe_2$ can be described by the Stoner model (Stoner 1938, Herring 1966). Thus we ignore the contribution of spin fluctuations. In the Stoner model the only excitations are single-particle excitations and the bands are rigidly split by an energy ΔE given by

$$\Delta E(B) = IM(B) + 2\mu_B B \tag{3}$$

where I is the effective exchange interaction and $M(B)$ is the magnetisation.

The splitting of the DHVA frequencies from the Onsager relation in equation (2) is

$$\Delta F = (\hbar/2\pi e)(\mathrm{d}A/\mathrm{d}E)\Delta E = (m_b/2\mu_B)\Delta E \tag{4}$$

where we have used $\mu_B = e\hbar/2m_0$ and the reduced band mass $m_b = (\hbar^2/2\pi m_0)\,\mathrm{d}A/\mathrm{d}E$.

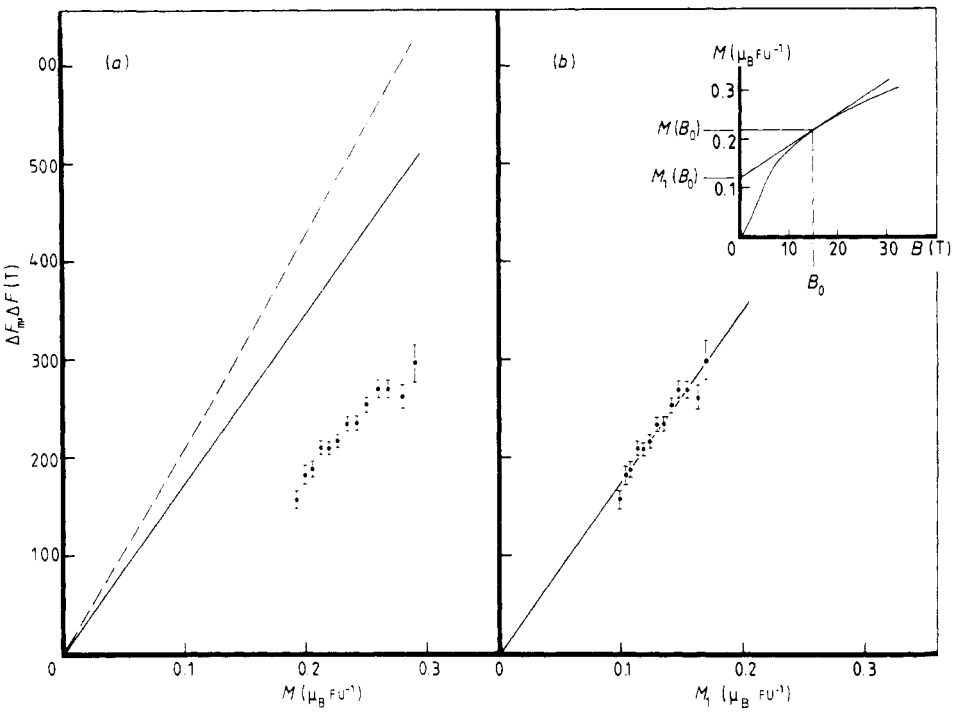

Figure 6. (*a*) The momentary frequency difference ΔF_m (full circles) plotted as a function of M. This was corrected for the 'Doppler' shift and the resulting ΔF is also given (full line). The slope of the ΔF against M plot is the same as the slope of ΔF_m against M_1 (figure 6(*b*)). The broken line is ΔF from the band-structure calculation. (*b*) The momentary frequency difference as a function of M_1. ΔF_m is found to be proportional to M_1 within the experimental error. The accuracy of the M_1 values is about 4%. The inset shows the relation between M and M_1 at some field B_0.

Substituting equation (3) in equation (4) and using the 'Doppler' equation (1) we have, for the momentary frequency difference,

$$\Delta F_m = (m_b I/2\mu_B)(M - B(dM/dB)) = (m_b I/2\mu_B)M_1 \tag{5}$$

which defines M_1. In the inset to figure 6 the relation between M and M_1 is illustrated. $M_1(B_0)$ is the intercept of the tangent to $M(B)$ in B_0 with the vertical axis. The Zeeman contribution to the energy splitting of equation (3) and thus to ΔF in equation (4) is completely cancelled in ΔF_m by the Doppler shift.

The values for M_1 can be readily obtained from the magnetisation data using the extrapolation of the linear part of the Arrott plot as describe above. In figure 6(*b*) ΔF_m is plotted as a function of M_1. We find that our results are well described by the linear relation

$$\Delta F_m = \alpha + \beta M_1 \tag{6}$$

where

$$\alpha = (0 \pm 2) \times 10^1 \text{ T} \qquad \beta = (1.7 \pm 0.2) \times 10^3 \text{ T}/\mu_B,$$

in agreement with the Stoner model.

6.3. Discussion of the results for ΔF_m

The Onsager ΔF follows by substitution of equation (3) in equation (4):

$$\Delta F = (m_b I/2\mu_B)M + m_b B = \beta M + m_b B. \tag{7}$$

This is also plotted in figure 6(*a*) using the constant β from equation (6). There is a difference of about 25% between the experimental and theoretical values for the slope of ΔF as a function of M. For an estimate of the constant β from the band-structure calculation we assume that the DOS, $N(E)$, is constant near E_F. At sufficiently low temperatures we have

$$M = N(E_F)\Delta E. \tag{8}$$

Combining this with equation (4) gives

$$\Delta F = (m_b/2\mu_B N(E_F))M. \tag{9}$$

Thus from the band-structure calculation we have

$$\beta_{calc} \simeq m_b/2\mu_B N(E_F).$$

This is a rough approximation but it shows that the 25% difference with the experiment could be due to a calculated value for $N(F_F)$ which should be higher or a value for m_b which should be lower. Alternatively, this difference can be explained if we abandon the assumption of a rigid band splitting. The effective exchange interaction I may depend on the wavevector $\boldsymbol{k}$, so the measured energy splitting of the Γ orbits may be smaller than the effective splitting of all bands.

Table 2 lists values for ΔF_m and ΔF at different field strengths, using equation (7). We may define an effective Stoner factor S' for the Γ orbit and for different fields with

$$S' = \Delta E/2\mu_B B. \tag{10}$$

The values for S' are also listed in table 2. It can be seen here that with decreasing field S' tends to the usual Stoner factor

$$S = \chi_0/\chi_{Pauli} = \chi_0/2\mu_0\mu_B^2 N(E_F)$$

which for our material, with the experimental value for χ_0 and the calculated $N(E_F)$, has the value 59. This must be so, for with equation (8) one can show that $S' = S$ for vanishing field strengths. Yet the 25% difference between the experimental and theoretical values for β leads to a 25% difference in the values for $S'(B = 0)$ and S.

The fact that a Stoner relation between ΔF_m and M_1 is found corresponds to the fact that the Arrott plot is linear for the field values studied. Below 10 T the Arrott plot is curved and, if spin fluctuations influence the magnetisation, we may expect to find a

Table 2. Some values for ΔF_m and derived quantities for the Γ orbit along [110]. ΔE is found from ΔF using equation (4). The definition of S' is given in the text.

B(T)	$M(\mu_B)$	ΔF_m(T)	ΔF(T)	ΔE(mRyd)	S'
22.1	0.260	270 ± 9	450 ± 50	6.3 ± 0.7	34 ± 4
18.8	0.242	235 ± 7	420 ± 50	5.9 ± 0.7	37 ± 4
15.0	0.219	209 ± 7	380 ± 50	5.3 ± 0.6	42 ± 5
12.2	0.199	182 ± 9	350 ± 40	4.8 ± 0.6	46 ± 6

deviation from the linear dependence of ΔF_m on M_1. Note here that $M_1 = 0$ at the field where the susceptibility is at its maximum, i.e., at a field of about 6 T. Experiments in fields below 10 T are in preparation.

7. Conclusion

The DHVA frequencies in $TiBe_2$ above 10 T are well described by two sheets of Fermi surface showing a ferromagnetic-like splitting. Only orbits having a relatively light mass are observed and they are used as a probe for the magnetisation caused by the heavy bands.

A large value for the mass enhancement for the Γ orbit is observed, in agreement with high-field specific heat data, whereas for the X orbit the enhancement is half that value. Spin fluctuations will affect the dressing of the electrons and it is interesting to look for field and temperature dependences of the effective masses.

The exchange splitting of the Γ orbit is proportional to the magnetisation in fields between 11 and 30.4 T, in agreement with the Stoner model. In fields below 10 T a departure from the linear dependence of the exchange splitting on the magnetisation may be observed.

Acknowledgments

We thank H M Weijers for his technical assistance, Dr R W van der Heijden for his assistance in the magnetisation measurements and Dr T Jarlborg for discussions. Part of this work was supported by the Stichting voor Fundamenteel Onderzoek der Materie and the United States Department of Energy.

Appendix

The traditional muffin-tin approximation actually involves two approximations: the potential within the muffin-tin (MT) spheres is spherically averaged and the potential in between the MT spheres is considered to be constant. The latter approximation was not applied in the earlier calculation on $TiBe_2$ (de Groot *et al* 1980): non-muffin-tin corrections were included through the Fourier coefficients of the potential ('warped muffin-tin approximation'). Non-spherical terms in the potential inside the MT spheres were not taken into account in the earlier paper. The size of these corrections is expected to be small and their influence modest: they will influence the position of the t_{2g} Ti d electrons compared with the e_g Ti d electrons but will not influence the Be s electrons or the Ti s and p electrons. That the size of the correction is to be small stems from the fact that the Be sublattice charge density does not contribute to the non-spherical terms in the Ti potential (de Groot and Janner 1984). The dominant correction is due to the nearest-neighbour Ti atoms. The shape and size of the X_7 DHVA orbit are very sensitive to non-spherical corrections within the Ti muffin-tin spheres as will now be shown.

Let us focus on the electronic structure at the point X. Bands 7 and 8 form a doublet at X of pure t_{2g} symmetry, and bands 9 and 10 a doublet of pure e_g symmetry (t_{2g} and e_g are not to be considered here as symmetry labels but as a label meaning t_{2g} being comprised of d_{xy}, d_{xz} and d_{yz} orbits, and e_g being composed of d_{z^2} and $d_{x^2-y^2}$ orbits). Along the line z the

Table 3. The $\boldsymbol{k} \cdot \boldsymbol{p}$ Hamiltonian for bands 7–10 around the point X. For visual clarity only the upper half of the Hamiltonian is shown and all coefficients except p_1 and p_2 have been omitted. The component of $\boldsymbol{k}$ along x is denoted by x, etc.

$p_1 + z^2 + x^2 + y^2$	$-z + \mathrm{i}xy$	$\mathrm{i}y + xz$	$-\mathrm{i}x - yz$
—	$p_1 + z^2 + x^2 + y^2$	$x + \mathrm{i}yz$	$-y - \mathrm{i}yz$
—	—	$p_2 + z^2 + x^2 + y^2$	xy
—	—	—	$p_2 + z^2 + x^2 + y^2$

t_{2g} doublet gently curves down and at the intersection with the Fermi energy the wavefunction character of band 7 has mainly t_{2g} symmetry. Along Δ (and S), however, the band 9–10 doublet splits rapidly. Close to X the lowest e_g state crosses the t_{2g} states. As a consequence the wavefunction of the intersections of band 7 with the Fermi energy along Δ (and S) is primarily of e_g character. Thus any inaccuracy in the positions of the e_g electrons compared with the t_{2g} electrons will be reflected directly in the shape and size of the X_7 orbit. On the other hand, an accurate knowledge of the shape and size of the X_7 orbit will allow us to determine the size of the non-muffin-tin correction!

In order to do this the four bands (7–10) were fitted to a $\boldsymbol{k} \cdot \boldsymbol{p}$ Hamiltonian around X. A fit of the coefficients of a second-order $\boldsymbol{k} \cdot \boldsymbol{p}$ Hamiltonian shown in table 3 to the original LAPW bands was performed; the RMS error of the fit was better than 0.1 mRyd. Two constants appear on the diagonal of the $\boldsymbol{k} \cdot \boldsymbol{p}$ Hamiltonian, called p_1 and p_2 in table 3. Their physical meaning is the position of the doublets at X. It is exactly those parameters, or more specifically their difference, which is determined by the non-spherical terms in the potential in the Ti spheres. This energy difference was varied to give the best agreement with the observed branches of the X_7 orbit, taking the average of spin-up and spin-down values. The result was a non-muffin-tin correction of 6.4 mRyd. However, such a correction cannot be applied without a correction to the Fermi energy: the lowering of the lowest doublet at X will also suppress the Fermi energy somewhat. This correction is more difficult to obtain, since the $\boldsymbol{k} \cdot \boldsymbol{p}$ fit has only local validity and cannot be used for the Brillouin-zone integration needed for the determination of a new Fermi level. A shift of 2.7 mRyd seems reasonable, however, and also brings the Γ_{10} orbit into very close agreement with experiment. Higher-order non-muffin-tin corrections are of less importance and will, for example, influence the position of the upper branch of the X_7 orbit near the [001] direction most. Since only four points could be obtained here experimentally, no attempts were made to obtain higher-order non-muffin-tin corrections.

References

Acker F, Fisk Z, Smith J L and Huang C Y 1981a *J. Magn. Magn. Mater.* **22** 250–6

Acker F, Huguenin R, Pelizzone M and Smith J L 1981b *Phys. Rev.* B **24** 5404–6

Acker F, Huguenin R, Smith J L and Huang C Y 1982 *J. Physique Lett.* **43** L205–9

Alloul H and Mihaly L 1982 *Phys. Rev. Lett.* **48** 1420–3

van Deursen A P J, van Ruitenbeek J M, Verhoef W A, de Vroomen A R, Smith J L, de Groot R A, Koelling D D and Mueller F M 1982 *Physica* B **109–110** 2159–61

van Deursen A P J and de Vroomen A R 1984 *J. Phys. E: Sci. Instrum.* **17** 155–9

Enz C P and Matthias B T 1979 *Z. Phys.* B **33** 129–33

Giorgi A L, Matthias B T, Stewart G R, Acker F and Smith J L 1979 *Solid State Commun.* **32** 455–8

Gold A V 1968 *Solid State Physics* ed. J F Cochran and R R Haering (New York: Gordon and Breach) pp 39–126
de Groot R A and Janner A G M 1984 to be published
de Groot R A, Koelling D D and Mueller F M 1980 *J. Phys. F: Met. Phys.* **10** L235–40
Herring C 1966 *Magnetism* vol. 4 ed. G T Rado and H Suhl (New York: Academic)
Jarlborg T and Freeman A J 1980 *Phys. Rev.* B **22** 2332–42
Jarlborg T, Freeman A J and Koelling D D 1981 *J. Magn. Magn. Mater.* **23** 291–8
Jarlborg T, Monod P and Peter M 1983 *Solid State Commun.* **47** 889–93
Lonzarich G G, Sigfusson T I, Bernhoeft N R, Buiting J J M, Mueller F M and Kübler J 1984 to be published
Matthias B T, Giorgi A L, Struebing V O and Smith J L 1978 *Phys. Lett.* **69A** 221
Monod P, Felner I, Chouteau G and Shaltiel D 1980 *J. Physique Lett.* **41** L511–3
van Ruitenbeek J M, Verhoef W A, Mattocks P G, Dixon A E, van Deursen A P J and de Vroomen A R 1982 *J. Phys. F: Met. Phys.* **12** 2919–28
Stewart G R, Smith J L and Brandt B L 1982b *Phys. Rev.* B **26** 3783–7
Stewart G R, Smith J L, Giorgi A L and Fisk Z 1982a *Phys. Rev.* B **25** 5907–17
Stoner E C 1938 *Proc. R. Soc.* A **165** 372–414
Wohlfarth E P 1980 *J. Physique Lett.* **41** L563–5
—— 1981 *Comm. Solid State Phys.* **10** 39